npj | gut and liver

Review

https://doi.org/10.1038/s44355-025-00035-x

Surgical optomics: a new science towards surgical precision

Gabriel Szydlo Shein[1,10], Elisa Bannone[2,3,10], Silvia Seidlitz[4,5], Mohamed Hassouna[6], Luca Baratelli[7], Arturo Pardo[7], Sylvain Lecler[1,8], Frédéric Triponez[9], Manish Chand[6], Sylvain Gioux[7], Lena Maier-Hein[4,5] & Michele Diana[1,9] ✉

Surgical Optomics represents the convergence of optical imaging technology and advanced computational analytics to create a new paradigm for precision surgery. Key techniques include fluorescence-guided surgery (FIGS) using exogenous dyes, spectral imaging leveraging endogenous chromophores (e.g., hemoglobin, water), and Single Snapshot of Optical Properties (SSOP) for real-time quantitative imaging. This study examines the potential and limitations of some current Surgical Optomics technologies, aiming to advance understanding and foster innovation in this transformative field. By turning the operating room into a data-rich environment, this field has the potential to revolutionize surgical care, enabling better outcomes for patients.

The quest for advanced intraoperative diagnostic and therapeutic tools has spanned centuries, but only with the recent surge in Big Data and Artificial Intelligence has a truly effective solution become feasible[1].

Recent decades have seen significant advances in optical technologies for surgery[2]. Initially, efforts focused on bridging the gap between human vision and imaging systems, progressing from Standard Definition (SD) to High Definition (HD), 4 K, and 3D imaging. As technology evolved, the focus shifted toward surpassing human vision— achieving microscopic visualization, and revelation of the previously invisible. In other words, the surgical augmented eye[3].

This evolution has given rise to *surgical optomics*[4], an emerging interdisciplinary field that pairs optical imaging technology with advanced computational methods to provide relevant, real-time, quantitative, and functional information during surgical procedures. "Omics" refers to the comprehensive characterization and quantification of biological systems[5]. Surgical optomics applies this approach to enable surgeons to quantitatively assess tissue composition and pathophysiological properties (e.g., perfusion, hydration), at both the micro- and macroscopic level, with unprecedented precision. In providing real-time access to previously unattainable data, Surgical Optomics has the potential to enhance intraoperative decision-making, yet the scope, applications and limitations of surgical optomics remain underdefined. We aim to delineate this emerging field by exploring the most prevalent and widely available surgical optical imaging techniques, as well as those with significant potential for future advancements (Fig. 1).

The electromagnetic spectrum – how different wavelengths are leveraged for surgical use

The electromagnetic spectrum refers to the full range of electromagnetic radiation characterized by wavelength or frequency. The wavelengths visible to humans (400–780 nm) represent only a small portion of this continuum, which encompasses every type of energy wave[6]. From long, slow, and low-energy radio waves to ultra-short, fast, high-energy gamma rays, the spectrum contains seven broad classes based on how these waves behave when interacting with matter[7] (Fig. 2).

Although every class in the electromagnetic spectrum has been applied in the medical field, Surgical Optomics focuses on wavelengths within the ultraviolet, visible, and infrared light ranges (approximately from 300 to 3000 nm), offering a cost-effective, high-resolution imaging without the use of ionizing radiation[8].

By studying the interaction between light and matter, it is possible to understand how different electromagnetic wavelengths behave when propagating through various biological tissues — how each one is absorbed, reflected, and refracted in distinct settings (Fig. 3). This enables the characterization of tissue molecules and facilitates objective clinical conclusions[9].

This study examines the most prevalent and promising surgical optical imaging techniques, emphasizing their current applications and potential for future advancements. The analysis is categorized into two primary approaches: exogenous fluorescence, represented by fluorescence-guided surgery, which utilizes externally administered contrast agents for enhanced

[1]Laboratoire des Sciences de l'Ingénieur, de l'Informatique et de l'Imagerie (ICUBE), University of Strasbourg, Strasbourg, France. [2]Research Institute against Digestive Cancer (IRCAD), Strasbourg, France. [3]Department of Hepato-Bilio-Pancreatic Surgery- P. Pederzoli Hospital, Peschiera Del Garda, Verona, Italy. [4]Division of Intelligent Medical Systems (IMSY), German Cancer Research Center (DKFZ), Heidelberg, Germany. [5]Helmholtz Information and Data Science School for Health, Heidelberg/Karlsruhe, Germany. [6]Division of Surgery and Interventional Science, University College London, London, UK. [7]Intuitive Surgical, Geneva, Switzerland. [8]Institut National des Sciences Appliquées (INSA) Strasbourg, Strasbourg, France. [9]Department of Surgery, University of Geneva, University Hospitals of Geneva, Geneva, Switzerland. [10]These authors contributed equally: Gabriel Szydlo Shein, Elisa Bannone. ✉e-mail: michele.diana@insead.edu

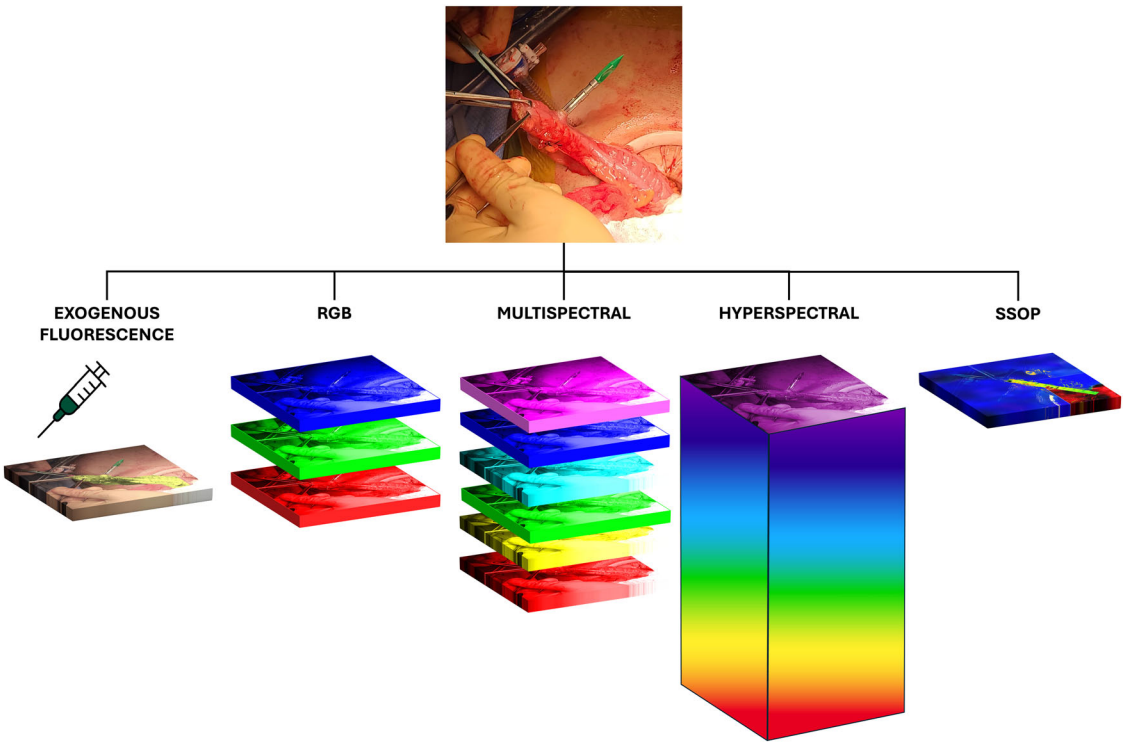

Fig. 1 | Schematic representation of key technologies in Surgical Optomics.

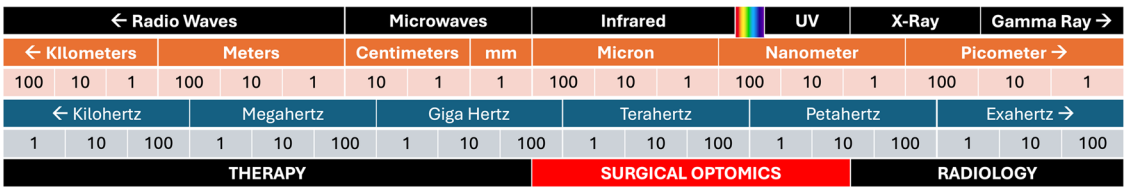

Fig. 2 | Diagram of the electromagnetic spectrum. Orange stripe display wavelengths, which increase in length towards the left. Blue stripe display frequency, which is inversely proportional to wavelength (decreasing towards the left). Surgical Optomics primarily focuses on wavelengths within the range between infrared and ultraviolet, including the visible spectrum.

visualization[10], and endogenous fluorescence, including hyperspectral imaging and spatial frequency domain imaging (SSOP), which exploit intrinsic tissue properties to provide functional and structural insights[9]. This framework aims to elucidate the advantages, limitations, and future prospects of these modalities in advancing surgical precision and outcomes.

Exogenous fluorescence

Principle

Fluorophores are chemicals that can absorb light at a specific wavelength and re-emit it at a typically higher (lower energy) wavelength. Fluorescent imaging exploits this physical phenomenon by utilizing spectrally resolved light sources that excite the injected exogenous fluorescent dye, which in turn emits a signal. This signal is detected by cameras equipped with light-collection filters and processed through specialized hardware and software, ultimately displaying the fluorescent data, potentially superimposed on a white-light illuminated image.

By administering these fluorophores in Fluorescence Guided Surgery (FIGS), specific structures that would otherwise be indiscernible to the naked eye can be set apart from their surroundings, giving the surgeon critical support for adequate real-time decision-making[11].

Each fluorophore used in FIGS has specific optical and pharmacokinetic characteristics that allow for its use in different situations. Among the clinically available fluorophores, those that emit light in the Near Infrared (NIR) wavelength spectrum (700–1700 nm) are of special interest for translation into surgical practice because the signal at this wavelength can penetrate deeper into tissues with less photon absorption, scattering, or auto-fluorescence, resulting in high-contrast, three-dimensional data[12–14].

Clinical application

Since its first use nearly a century ago[11], fluorescence in surgery has proven to be a real-time, dynamic, easy-to-use, non-invasive, low-toxicity, and low-cost way to obtain otherwise invisible data in both open and minimally invasive surgery[10]. Clinically approved FIGS uses non-targeted fluorescent contrast agents such as indocyanine green (ICG) and methylene blue (MB)[1,4,15], which allow for multiple applications, including surgical navigation, structure identification, tumor delineation, and metabolic activity evaluation[3,16].

Fluorescence can be applied dynamically—imaging an area over time to draw clinical conclusions—or statically, using a single image to evaluate the fluorescence intensity of a specific area relative to the background or other areas. The amphiphilic nature of ICG allows it to bind to plasma proteins, achieving uniform blood distribution when injected intravenously. This makes it ideal for real-time, dynamic perfusion assessment[17,18], as demonstrated by several clinical trials on fluorescence guided angiography (FA), including in gastrointestinal surgery (e.g., anastomosis evaluation)

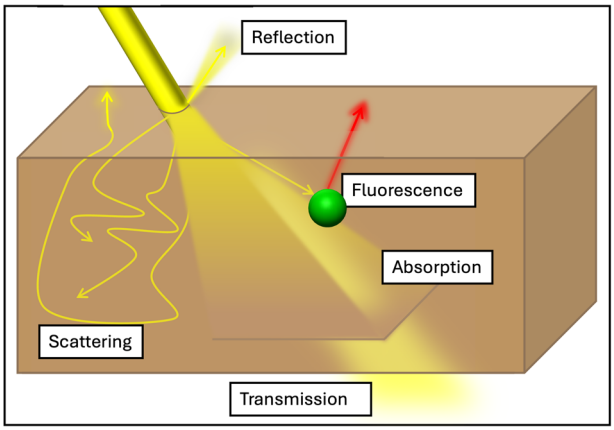

Fig. 3 | Schematic of light tissue interactions. Absorption occurs when light is absorbed by tissue molecules and converted into other forms of energy (e.g., heat). Reflection refers to light bouncing specularly (at a single angle) off the surface. Scattering involves deflection of light in various directions by tissue structures (e.g., organelles and fibers) which may also alter the photon's wavelength. Fluorescence is the re-emission of absorbed light at a different wavelength. Transmission describes the process of photons passing through tissue without being dissipated. These phenomena occur simultaneously and at varying degrees depending on tissue properties and light characteristics.

and transplant surgery (e.g., vascular patency and real-time liver perfusion monitoring[15,19–25]).

ICG has also advanced oncological surgery for lymph node mapping and tumor detection. In 2005 Kitai et al. demonstrated its feasibility for lymph node visualization in breast cancer[26]. Subsequent studies showed it to be as effective as existing alternatives while being less disruptive to surgical workflow and free of ionizing radiation[27,28]. Fluorescent dyes are also valuable for lymph node mapping in gastrointestinal procedures, such as esophageal, gastric, and colonic surgeries[29–31]. Nonetheless, dose, volume, and injection methods remain topics of discussion[32]. Tumor detection applications often rely on passive fluorophore diffusion into tumors via aberrant vasculature, pharmacodynamic properties of the fluorophore, or the binding of fluorescent probes to targeted ligands[33,34]. Off label, ICG has been used to visualize various cancers, including liver, breast, colorectal, head and neck tumors, and melanoma[28,35–38].

Liver applications of ICG have been extensively studied due to its hepatic metabolism[35,39]. Hepatocellular carcinomas emit a strong fluorescent signal due to impaired biliary excretion[40], while liver metastases exhibit a fluorescent ring from healthy immature hepatocytes surrounding the tumor, attributed to downregulation of anion transporters[41]. ICG hepatic metabolism also enables real-time identification of extrahepatic biliary structures without radiation[42], potentially reducing operative time and laparoscopic-to-open conversion rates, though its impact on postoperative complications remains unproven[43,44]. Finally, ICG is used to demarcate anatomical boundaries in segmental hepatic resections. It guides parenchymal delineation through both positive and negative staining techniques, enabling precise surgery while preserving healthy liver tissue[45].

In recent years, several large-scale clinical trials and systematic reviews have underscored the clinical value of ICG-based perfusion assessment across a range of surgical applications. The EssentiAL trial, a phase III randomized study with 839 patients undergoing minimally invasive rectal surgery, demonstrated that intraoperative ICG fluorescence angiography reduced anastomotic leak rates by 4.2% (RR 0.645, 95% CI 0.422–0.987; $p = 0.041$)[46]. Multiple recent meta-analyses of ICG use in colorectal surgery have consistently reported a significant reduction in anastomotic leak risk (pooled relative risks ≈0.5 and NNT 22–23)[47–50]. Similarly, for oncologic liver resection, different meta-analyses (with sample sizes of 417 to 1260) have consistently concluded that ICG guidance significantly decreases operative time (by 16–21 min), intraoperative blood loss (~100 mL), hospital stay (~1–1.6 days), and postoperative complications, with a significantly higher one-year disease-free survival (OR 2.87) relative to non-ICG controls[51,52]. Beyond these oncological applications, ICG has been increasingly leveraged in the field of Liver Transplant for graft evaluation, donor safety, and anatomical guidance, as shown in a review by Lau et al. which demonstrated that ICG clearance during normothermic machine perfusion can reliably predict early allograft dysfunction and correlates with postoperative outcomes, while intraoperative ICG angiography provides real-time assessment of arterial, venous, and biliary patency[20]. Recent clinical studies have applied ICG cholangiography during donor hepatectomy to delineate biliary anatomy, demonstrating that the use of ICG reduces biliary complications relative to historical rates, improves precision in bile duct transection[53,54], leads to faster biliary anastomosis (mean time 28 vs. 37 min, $p = 0.02$) and fewer postoperative biliary leaks (2.5% vs. 8.3%, $p = 0.04$)[55].

Open challenges

FIGS has demonstrated its value as a tool that provides surgeons with supplementary, previously invisible information for clinical decision-making. Despite the growing adoption of fluorescent contrast agents in clinical practice and their injection generally being regarded as safe, rare but severe complications, such as anaphylactic shock, have been reported[56,57]. Furthermore, prolonged washout times of fluorescent contrast agents, such as 30 min for ICG[58]) pose challenges for the repeated testing required in applications like perfusion monitoring.

Current clinically approved fluorescence systems cannot provide quantitative results because they fail to measure the absolute concentration of fluorescent agents in tissues and lack control over basic variables that affect signal readings[59]. Fluorescence intensity directly varies with the square distance between the tissue and the imaging system. Without rigorous control or normalization, the observed signal cannot reliably indicate actual perfusion[60–63]. Additionally, each commercial system uses proprietary algorithms with unique cutoff values, rendering results from different systems mostly incomparable[64,65]. Fluorescence signals may appear blurry or lack resolution due to light scattering within the tissue. The attenuation of both excitation light and fluorescence emission hinders accurate localization and quantification of fluorescence, which is essential for precise and quantitative diagnostic applications. As a result, surgeons rely only on qualitative images, leading to subjective, inconsistent, and biased interpretations[66,67]. Current evidence remains low and insufficient to recommend FIGS broadly for reducing surgical complications[36,68,69].

Efforts to achieve objective quantification have introduced methods such as signal-to-background-ratio (SBR), which compares the mean signal from target tissues to background fluorescence. SBR can provide pseudo-quantification and more standardized results[70]. Calibration devices like the Green Balance™ ICG Reference Card (Diagnostic Green; Aschheim–Dornach, Germany) and the CalibrationDISK™ (SurgVision BV, Harde, the Netherlands) can improve reproducibility by controlling variables such as camera distance and illumination, generating space-resolved pseudo-quantitative results in static images[71,72].

Time-resolved quantification has also been explored as an alternative to absolute fluorescence intensity parameters[73]. For instance, fluorescence-based enhanced reality (FLER) (Fig. 4) analyzes temporal fluorescence characteristics rather than the intensity of individual pixels, generating quantitative perfusion cartography that overlaid onto real-time laparoscopic videos. These color-coded maps, which highlight varying levels of tissue perfusion, offer more clinically valuable insights compared to traditional qualitative ICG systems[61,62,74]. Although FLER has shown experimental[60–63,75–77] and clinical[78] accuracy, its implementation remains time-consuming and adds complexity to surgical workflows[79]. Repeated analyses encounter the same issues observed with standard ICG assessment. Other approaches that rely on time-resolved metrics (e.g., time to peak, maximum fluorescent value over time, slope of the time to peak), face challenges due to the lack of standardized variables, leading to heterogeneous results preventing standard implementation in clinical practice[80].

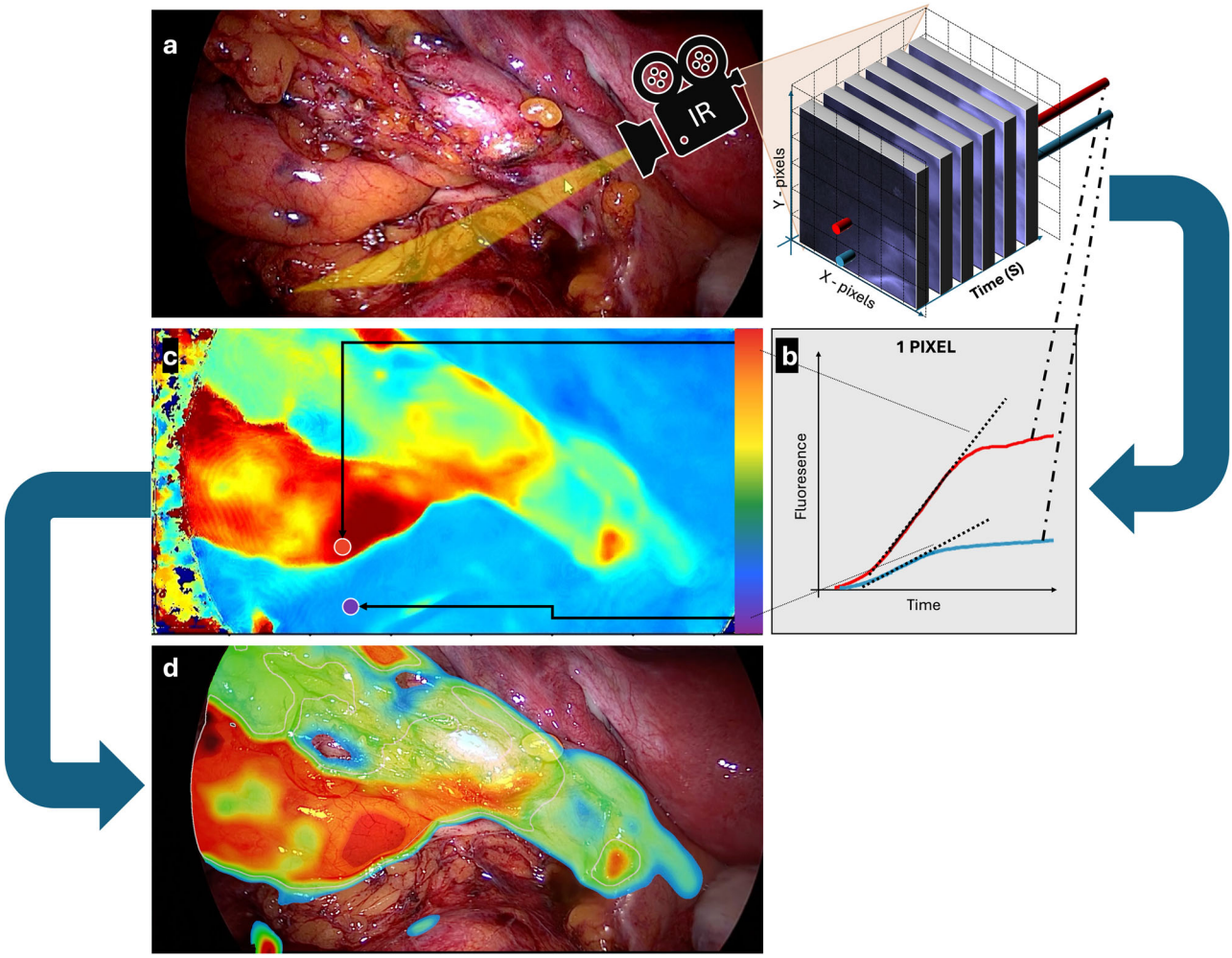

Fig. 4 | FLER system used in a left hemicolectomy. a After ICG is injected and recorded over time with an infrared camera (**b**) Fluorescence Time to Peak is computed (**c**) and a virtual perfusion cartography is built (Red = High time to peak ∴ low perfusion). **d** The virtual cartography is superimposed onto real-time images to obtain a mixed reality effect and display the quantified ICG signal directly on the bowel.

Machine learning algorithms have shown promise in fluorescence analysis, reducing subjectivity by identifying dynamic intensity patterns over time. These algorithms can distinguish between cancerous and normal tissue with minimal disruption to surgical workflow[81]. The ongoing CLASSICA project uses machine learning to analyze ICG perfusion patterns, aiming at differentiating benign and malignant rectal polyps[82]. However, these analyses are conducted in the postoperative period and are not available in real time during surgery.

Targeted fluorescent agents represent another frontier in the advancement of FIGS, aiming to overcome current limitations of oncologic applications and enable real-time analysis. These fluorescent probes typically use a biomarker conjugated to a fluorophore, thereby providing a signal at the target site and enabling real-time visualization of primary tumors, neoplastic lymph nodes, and distant metastasis[12,59]. Among the myriad fluorescent probes developed, antibodies and peptide-based recognition elements are of particular interest. Fluorophore-antibody probes, inspired by targeted cancer therapies, have demonstrated exceptional precision, with high sensitivity and specificity in detecting multiple tumors in both experimental settings[83,84] and clinical trials[85]. Similarly, fluorescent peptide probes rely on a labeled peptide sequence that can selectively bind to or become modified by the molecular target expressed at the tumor site, offering numerous advantages, including rapid distribution and reduced or absent immunogenicity[86]. The drawback is that each targeted probe is specific to a tumor and must undergo extensive development and navigate regulatory hurdles before clinical use. Additionally, as with non-targeted fluorophores, quantifying targeted fluorescence to correlate intensity with tumor characteristics remains a challenge. Targeted fluorescent agents have also been evaluated in endoscopic applications. Phase II and phase III trials[87,88] have demonstrated their feasibility for tumor identification, highlighting their potential as an alternative for endoscopic follow-up of esophageal and rectal lesions[89–91].

The limitations of non-targeted and targeted FIGS have spurred interest in alternative imaging technologies. While FIGS offers considerable benefits, its transition to a standard surgical tool requires addressing the lack of quantification, improving standardization, and navigating regulatory challenges for targeted agents.

Dye-free methods have been developed as alternative approaches for tissue characterization that do not require exogenous agents. Autofluorescence, which operates on the same optical principles as exogenous fluorescence but without the need for a contrast agent, has been extensively studied within FIGS. However, its application is limited to tissues with naturally occurring intrinsic fluorophores, such as the parathyroid[92,93]. Although effective for specific applications, autofluorescence is static and has a significantly lower signal-to-background ratio, which has hindered its development as a general alternative to exogenous fluorescence. In contrast, emerging dye-free techniques that exploit light-tissue interactions—such as reflectance and scattering—are offering new opportunities for tissue characterization. These methods provide safer, more reliable imaging solutions without the need for exogenous agents.

Spectral imaging

Principle

Spectral imaging (SI) refers to imaging techniques that capture multiple bands across the electromagnetic spectrum to determine tissue composition noninvasively. Unlike standard cameras, which use only three visible spectral bands (red, green, and blue — RGB), SI covers a broader range, often including spectral bands corresponding to both visible and invisible light[94] (Fig. 5). As different tissue types (e.g., different organs) have unique optical properties (e.g., absorption, reflection and scattering) at different wavelengths, SI can potentially recover their detailed molecular composition, even beyond the visible surface[95–97]. SI is classified based on the number of spectral bands captured and their spectral bandwidth. It can be broadly divided into multispectral imaging (MSI) and hyperspectral imaging (HSI). MSI typically captures up to tens of relatively broad, non-contiguous spectral bands using filters and illumination methods. HSI, in contrast, captures up to hundreds of narrow spectral bands per pixel, providing high spectral and spatial resolution[98].

Clinical application

Numerous image processing and machine learning algorithms have been developed to efficiently handle the large datasets of multidimensional images generated by hyperspectral cameras[99]. In surgical settings, both regression and classification algorithms have been exploited to extract clinically relevant parameters, ultimately providing valuable insights that can support surgical decision-making[100,101].

Regression techniques in SI. Regression techniques are employed to recover and quantify relevant functional tissue properties. This can be achieved using SI, as endogenous light-absorbing molecules in tissue - referred to as chromophores - absorb and scatter light at specific and known wavelengths in unique patterns[102–107]. Hemoglobin in blood is a key endogenous chromophore. SI leverages the distinct spectral signatures of oxygenated and deoxygenated hemoglobin to enable real-time imaging of tissue oxygenation and perfusion[108,109]. The quantification of functional tissue parameters has been applied across various clinical contexts, especially in colorectal surgery. This includes site selection for colon anastomosis[110,111], assessment of colon tissue vascularization[112], and the identification of optimal bowel transection points[113]. Recently, the authors developed the first real-time SI system that was applied in prospective patient studies[106].

Beyond tissue perfusion and oxygenation, regression-based SI can also monitor water distribution[114], serving as a sensitive and non-invasive tool for continuous, real-time monitoring of tissue hydration across diverse perioperative settings[115,116].

Classification techniques in SI. The unique composition of different tissue generates distinct spectral signatures, enabling precise intraoperative differentiation and characterization of specific organs and anatomical structures based on their "spectral fingerprints" (Fig. 6).

This ability of SI to distinguish between tissues in surgical settings was first demonstrated by Zuzak et al. during a laparoscopic cholecystectomy, where a near-infrared MSI system showcased the in vivo visualization of distinct anatomical structures[117]. Since then, SI has proven effective for anatomical navigation in a plethora of procedures, including thyroid surgery[118], neurosurgery[119,120], and liver surgery[121]. When integrated with advanced deep learning algorithms, SI enables automatic tissue recognition[122]. By classifying each pixel of a HS image, these models can automatically identify specific organs[123–125] and critical anatomical structures (e.g., biliary ducts, vessels, and nerves)[4,123–130]. This capability paves the way for real-time augmented reality applications and robotic automation in surgery, offering the potential to enhance precision in surgical interventions[4].

Cancer hallmarks, such as angiogenesis and increased metabolism, can alter hemoglobin and oxygen concentration, cellular structures, and vascular networks within tumor sites[131]. These tumor-associated changes can be leveraged by SI for various clinical purposes, including cancer tissue classification[122,132], metastasis detection[133–135], tumor site delineation[108,136], and sentinel lymph node identification across multiple tumor types[38]. Several studies have investigated hyperspectral imaging (HSI) for the non-invasive detection of colorectal cancer in freshly resected samples[135,136]. However, these studies are limited by small datasets or rely on classical machine learning models, such as support vector machines (SVMs) or multi-layer perceptrons (MLPs), which only consider spectral features smoothed with low-pass spatial filters, without employing deep learning techniques. Prior research on tissue classification[135,136] has shown that these traditional approaches without spatial smoothing, underperform compared to convolutional neural networks (CNNs)[122]. Ongoing studies are further exploring the applicability of MSI systems in the endoscopic setting, particularly, it is being evaluated by the authors for its ability to distinguish between normal and cancerous tissue in the colon and rectum based on their distinct optical signatures, without requiring intravenous contrast agents or tissue biopsy. Preliminary pre-clinical results have revealed clear spectral distinctions between healthy and pathological tissue in colorectal cancer specimens, further confirming the feasibility and safety of MSI in this context (Fig. 7).

In addition to the functional and structural mapping capabilities discussed above, HSI combined with machine learning can now be applied as a true theranostic tool. By guiding and assessing thermal damage during laser ablation therapies[137], HIS can reliably predicting both thermal thresholds

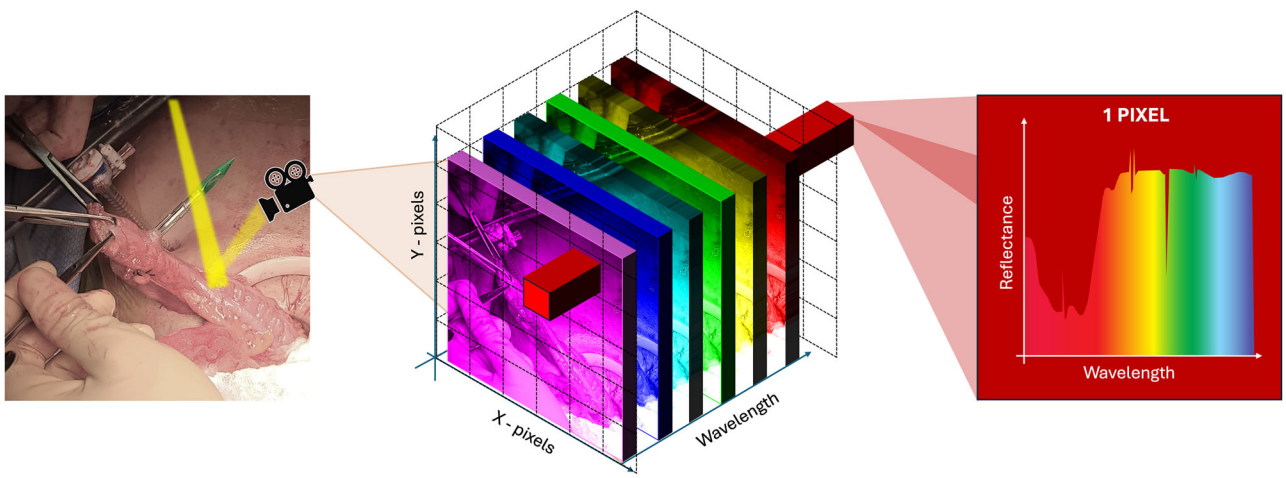

Fig. 5 | Schematic representation of a spectral imaging hypercube. SI acquires 3-dimensional data by measuring the tissue reflectance spectrum at each pixel.

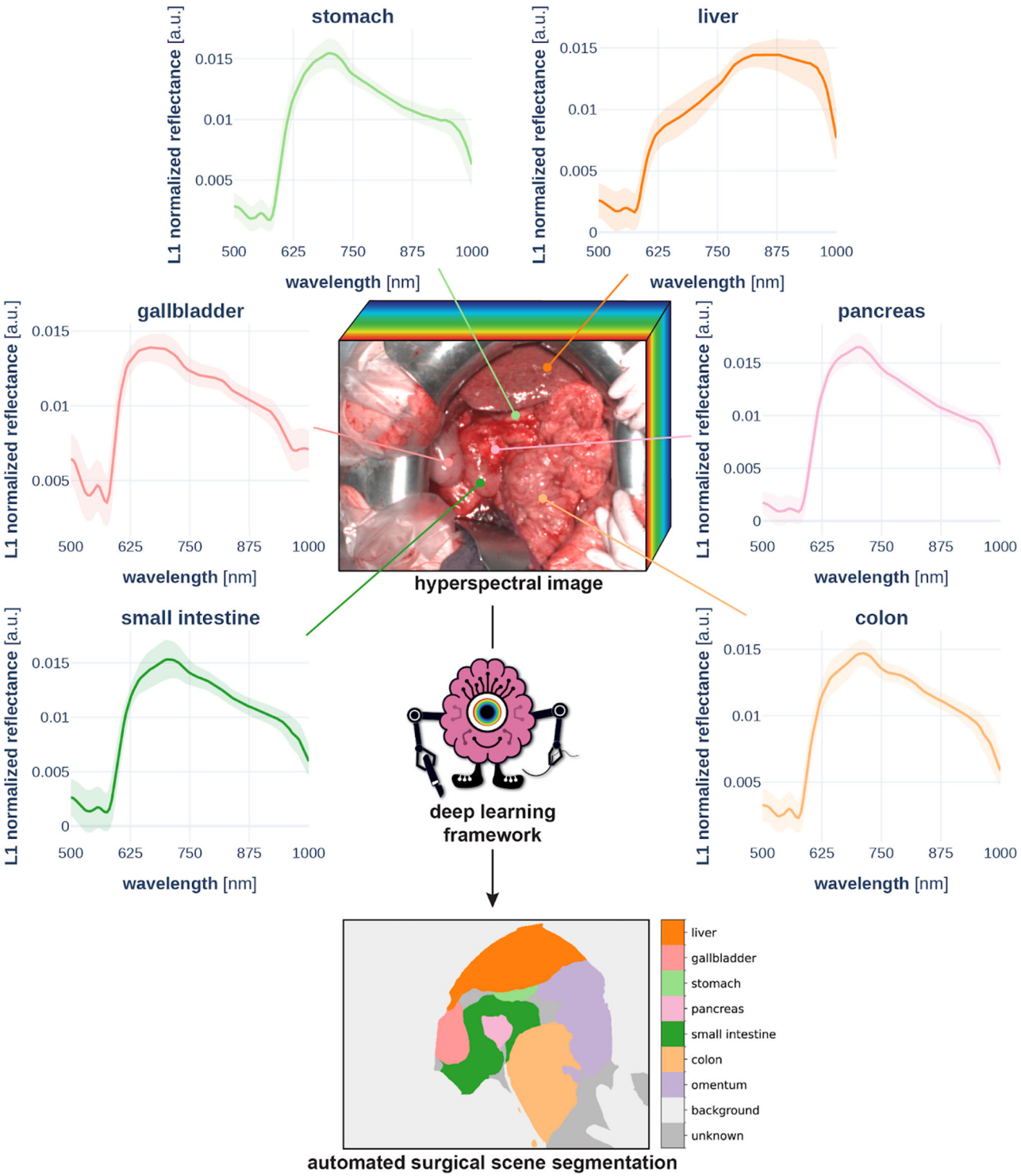

Fig. 6 | Automated surgical scene segmentation from hyperspectral imaging data. Human organs exhibit characteristic spectral profiles, which can be leveraged for highly accurate surgical scene segmentation using deep learning[116]. The plots show the median spectra (solid line) across gastrointestinal organ annotations for the sample image, with the shaded areas indicating the standard deviation.

and necrosis extent, with a strong correlation to histopathology scores[138] thus achieving high accuracy in delineating ablation margins during liver procedures in animal models[139].

There is growing evidence of the correlation between HIS and histopathological assessment. In the preclinical models of hepatic outflow obstruction, declines in HSI-derived oxygen saturation and rises in deoxyhemoglobin were spatially co-localized with histologically confirmed venous congestion and necrosis zones on H&E staining[121,140]. Additionally, in a clinical series of major hepatectomies, intraoperative HSI measurements were significantly correlated with post-operative serum markers of liver injury, which aligned with pathologically confirmed areas of ischemic damage[141].

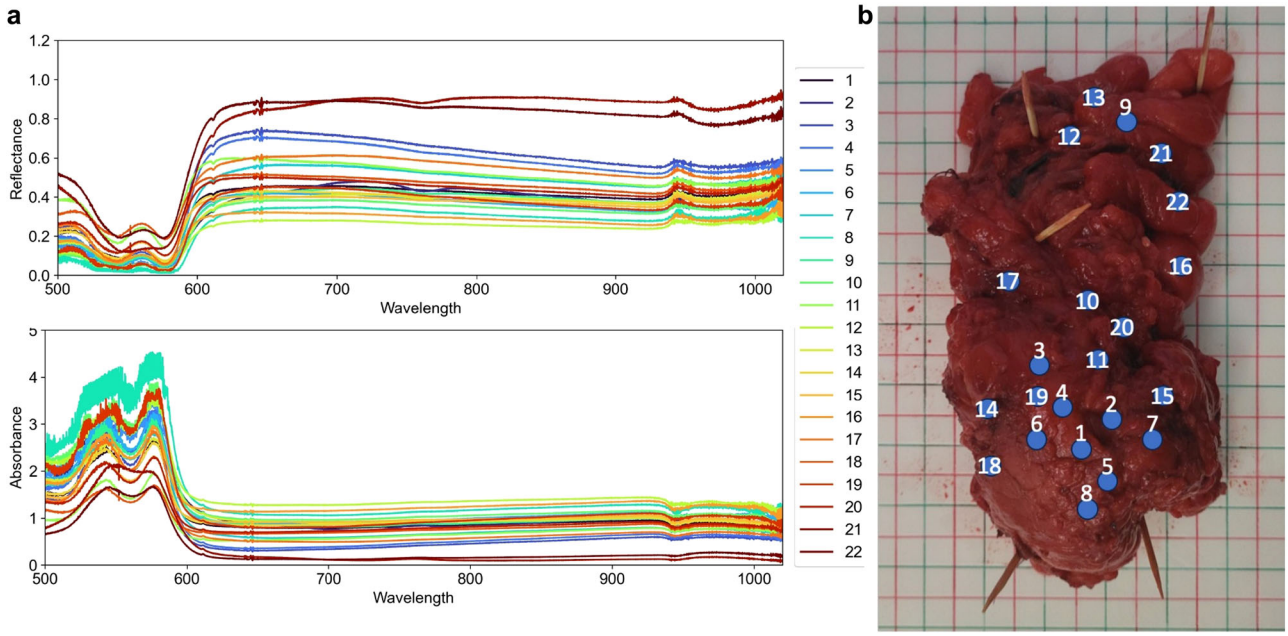

Fig. 7 | Hyperspectral data of a specimen of human colon with a tumor. **A** Representative spectral curve output generated by a commercially available hyperspectral camera. **B** Human colon specimen with regions of interest (ROIs) corresponding to colorectal cancer (#21, #22) and healthy tissue (ROIs #1–20). Absorbance and reflectance data are presented for wavelengths ranging from 500 to 1000 nm. The spectral curves are not normalized, which poses challenges for interpretation by clinical personnel. Close collaboration with data scientists is essential to derive clinically relevant insights for routine surgical practice.

Open challenges

While SI holds promise as a valuable intraoperative imaging tool, several challenges hinder its widespread adoption in clinical settings[142]. Limitations often emerge from the inherent challenges of balancing advances across all three critical dimensions of SI (spatial, spectral, and temporal resolution). Optimizing one dimension frequently necessitates trade-offs in the others, complicating efforts to achieve simultaneous and comprehensive improvements.

Quantitative imaging with SI faces significant challenges, including reproducibility and the robust quantification of functional tissue parameters. Current devices report non-quantitative chromophore indices (e.g., hemoglobin index) rather than clinically relevant tissue properties. These indices are generated using methods such as the Modified Beer-Lambert Law, time-domain diffuse spectroscopy, and second-derivative techniques, which have inherent limitations[143–146], including the reliance on unrealistic assumptions that do not hold in a clinical scenario or restricted applicability of the results to point measurements[147]. Machine learning approaches show potential[148] but require extensive annotated datasets and reliable reference gold standards — also defined as "ground truth" (e.g., blood gas analysis, or pathology), which remain scarce. Physics-based diffuse reflectance simulations for training machine learning algorithms[149–151] have equally shown potential but struggle with domain gaps and the lack of complex spatial context (i.e., limits in generating realistic spatially resolved maps of optical properties and simulating complex surfaces that include curvature or texture).

The scarcity of large, diverse medical HSI datasets further limits the development of robust deep learning algorithms. Most existing studies rely on single-center data, with only one known multicenter HSI study[4], and none to date exploring real-time applications. Although the number and size of medical HSI datasets are growing— some now encompassing tens to hundreds of patients[4,125,152] — few surgical HSI datasets are publicly available[120,153,154].

Device variability further aggravates these challenges. Parameters such as imaging methods (e.g., pushbroom, snapshot), number of spectral bands, spectral range, spectral and spatial resolution, sensitivity, and noise levels differ substantially across HSI devices[9,155]. Standardization is also lacking across file formats, accompanying metadata (e.g., exposure time, gain, environmental factors, clinical data), measurement protocols, and annotations. Such variability complicates cross-study validation and comparison.

Confounding factors remain mostly underexplored in medical HSI, yet they are critical to developing reliable deep learning models, preventing shortcut learning and algorithmic failure[156]. Seidlitz et al. have begun addressing this challenge by examining subject-, therapy-, and imaging-related confounders in automated sepsis diagnosis using HSI skin images[152]. For semantic surgical scene segmentation, recent studies have investigated model generalization across shifts in geometric domains[124,125], perfusion states[157] and illumination conditions[158].

Slow acquisition times also impede HSI integration into surgical workflows. Recent advances in high-speed spectral imaging devices for laparoscopic surgery show promise[109,159]. In open surgeries, dynamically changing lighting conditions necessitate continuous light source calibration, disrupting the surgical workflow and potentially compromising patient safety. Emerging techniques, such as those using specular highlights[160] or deep learning[158], aim to address inaccuracies in functional tissue parameter measurements and segmentation errors caused by uncalibrated illumination.

To advance SI adoption, multidisciplinary, well-designed, large-scale research initiatives are essential. These efforts should aim to identify the spectral characteristics required for specific diagnostic inquiries and establish which tissue types can be reliably differentiated. Future studies should prioritize capturing predefined spectral target structures, to streamline data processing and image acquisition. Additionally, tailored data extraction algorithms will be crucial to minimize delays between image acquisition and data availability, thereby enhancing the clinical utility of SI in surgical applications[142].

Single snapshot imaging of optical properties

Principle

While spectral imaging requires complex data processing to recover optical parameters from raw measurements Spatial Frequency Domain Imaging (SFDI) uses spatially modulated light patterns projected onto a tissue surface to directly probe its optical properties. By analyzing the reflected light at

different spatial frequencies, SFDI separates the effects of absorption and scattering, allowing for the extraction of quantitative optical properties (e.g., absorption coefficient, scattering coefficient) across the tissue.

Absorption is primarily dictated by the tissue's chemical composition, as photons can be absorbed by endogenous molecules, such as hemoglobin, lipids and water. In contrast, scattering arises from local variations in the refractive index and is influenced by cellular structural properties. These interactions are quantified as optical properties: the absorption coefficient and the scattering coefficient, respectively[161]. As a result, the absorption coefficient reflects the extent and nature of molecular interactions and is typically associated with functional metrics such as oxygenation, hydration or metabolism. In contrast, the scattering coefficient is related to sub-cellular structures, including nuclei, mitochondria, and collagen.

Single Snapshot of Optical Properties (SSOP) is an advanced imaging technique derived from SFDI that aims to simplify and speed up the process of acquiring optical property maps of tissues. Unlike traditional SFDI, which requires multiple spatially modulated patterns at different phase shifts and spatial frequencies, SSOP uses only a single spatially modulated illumination pattern to extract the tissue's optical properties. Advanced algorithms and pre-calibrations are used to compute tissue absorption and reduced scattering coefficients from just one image[162,163].

Clinical application

The measurement of optical properties, namely absorption and scattering coefficients, has been shown in the literature to highlight the presence of diseases or tissue alterations intraoperatively[164–171].

Technologies for measuring optical properties typically employ modulation techniques to resolve the temporal and spatial behavior of light propagation[161]. Most of these technologies require either a temporal sequence of images or a spatial scanning to measure and to generate optical properties maps, limiting their applicability for real-time intraoperative guidance. To address this limitation, SSOP was developed to provide quantitative measures of individual optical properties for each pixel in a wide field image within a single snapshot, thereby enabling real-time intraoperative imaging[172] (Fig. 8).

The SSOP technology was demonstrated preclinically in pigs to image oxygenation in real time using the Trident imaging system[173]. This technology was also validated in a variety of preclinical procedures in pigs, such as esophagus, liver, colorectal, stomach or kidney surgical procedures using metabolic biomarkers such as lactate for correlation[170,174,175]. Recently it was successfully translated to a clinical trial, where it was used to image the oxygenation of the externalized colon of 10 patients undergoing left anterior resection of the colon[78].

Open challenges

Current SSOP implementations, while enabling real-time optical property imaging with acceptable visual quality, face challenges such as edge artifacts and lower resolution compared to SFDI and spectral imaging. The integration of deep learning with Graphics Processing Units (GPU) computation and CNNs have enabled significant advances in biomedical optics, including achieving real-time processing despite network complexity. For instance, a study has demonstrated the feasibility of CNN-based, GPU-accelerated SSOP technology, which integrates 3D profile correction and high-quality image reconstruction from a single SSOP input.[172,176–178].

A preclinical in vivo trial highlights the capability of SSOP to generate real-time oxygenation rate maps, aligning with results from ICG fluorescence imaging. However, the simultaneous acquisition of oxygenation and fluorescence data has not yet been explored, and integrating or displaying both datasets concurrently could present technical challenges[173].

Currently, most studies have been conducted in preclinical settings using equipment that is neither commercially available nor widely accessible. The approval and adoption of the described technologies for clinical use will be essential to facilitate future clinical studies aimed at evaluating their impact on intraoperative surgical decision-making.

Future of surgical optomics

Surgical Optomics represents the convergence of optics, surgery, and computational analytics to create a new paradigm for precision surgery. By turning the operating room into a data-rich environment, this field has the potential to revolutionize surgical care, enabling better outcomes, reduced complications, and faster recovery for patients.

Emerging techniques in surgical optomics, currently in early preclinical development, hold significant promise for advancing intraoperative diagnostics.

Optical elastography is an advanced imaging modality that quantifies the biomechanical properties of biological tissues using light-based

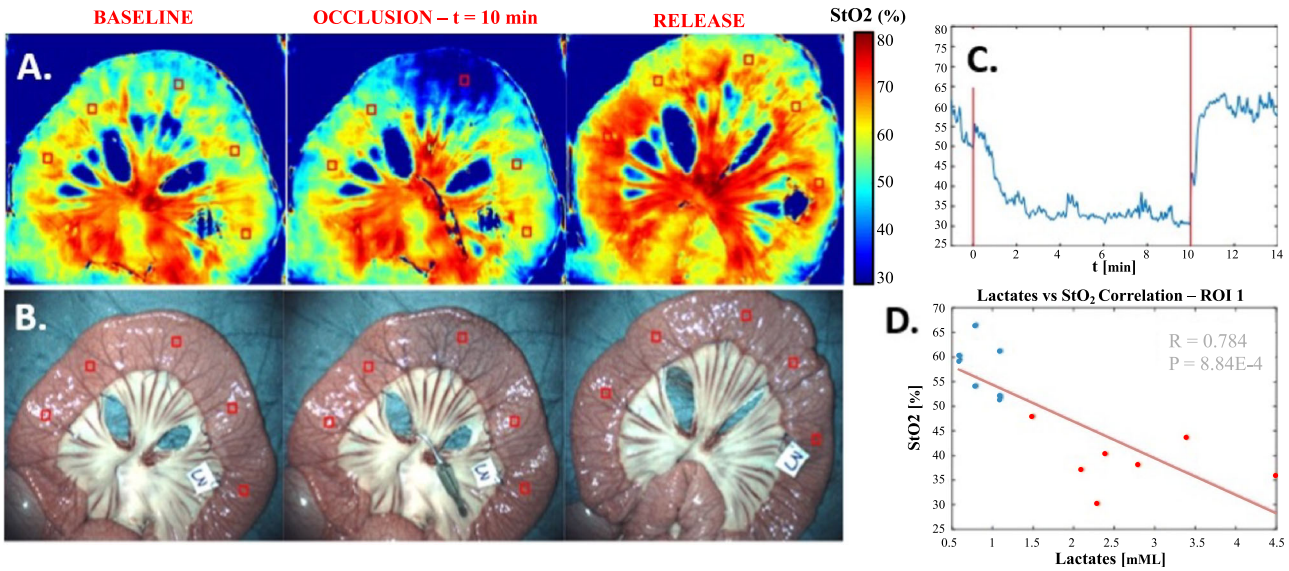

Fig. 8 | SSOP Preclinical results. A Oxygen saturation images of a swine bowel during baseline (t = −1 min), occlusion (t = 10 min), and after release (t = 14 min); (**B**) Corresponding color images; (**C**) Time course of occlusion measure at the center of the occlusion section; and (**D**) Pearson's correlation analysis between normalized lactates and SSOP-StO2 in correspondence to all ROIs. Of note capillary lactates were normalized according to systemic lactates to reduce variability. Lactates in ischemic ROIs (blue dots) were significantly higher compared to vascularized ROIs (red dots procedures) adapted from[172].

measurements. By leveraging the altered mechanical characteristics of pathological tissues compared to healthy ones, optical elastography has the potential to serve as a noninvasive intraoperative diagnostic tool[179].

Optical Coherence Tomography (OCT) is already utilized in some medical fields as a non-invasive imaging technique that produces high-resolution, cross-sectional images of biological tissues by measuring the backscattered light. Employing low-coherence interferometry with near-infrared light, OCT achieves varying tissue penetration depths based on optical properties. This technique provides micrometer-scale structural images, enabling detailed visualization and analysis of tissue morphology[180].

Full-Field Optical Coherence Tomography (FF-OCT), a variation of OCT, offers high-resolution, en face (surface-parallel) images rather than cross-sectional views. FF-OCT captures the entire field of view simultaneously, allowing for faster imaging over larger areas compared to conventional OCT. This technique is particularly suited for intraoperative pathology, where detailed surface imaging is essential for accurate tissue assessments. FF-OCT allows for real-time, label-free imaging, showing promise for identifying cellular and subcellular structures in tissue samples[181].

Intraoperative Raman Spectroscopy (RS) provides real-time molecular information of tissues during surgery by exploiting Raman scattering— a phenomenon where light interacts with molecular vibrations, resulting in wavelength shifts that reveal the molecular composition of tissues. This technique excels in distinguishing healthy tissues from diseased ones, such as differentiating cancerous from non-cancerous tissues, with exceptional precision[182].

All the cutting-edge imaging techniques discussed in this paper represent important progress in surgical optics; however, they remain experimental and require further development before clinical integration. Recent studies have begun to quantify clinical benefits, suggesting real potential for improving outcomes. For instance, ICG-guided lymphadenectomy in oncologic liver surgery improved 3-year disease-free survival from 68.2% to 81.4% (HR 0.53, $p = 0.012$)[183], and meta-analyses in colorectal surgery report significant reductions in intraoperative blood loss (WMD −4.38 mL, $p = 0.001$) and postoperative complications (WMD −0.04, $p = 0.027$)[184]. Moreover, multispectral and HSI tools have advanced beyond pilot feasibility and recent studies have demonstrated that real-time intraoperative oxygenation mapping is now practical, though integration into standard workflow remains an active area of development[101].

While technical feasibility has been demonstrated, routine clinical adoption will require overcoming implementation barriers. Future research will focus on assessing their clinical feasibility, cost-effectiveness, and potential to enhance diagnostic precision and support real-time surgical decision-making.

As detailed above, further important steps towards the advancement and implementation of surgical optomics in clinical practice are:

- Standardization and Validation: Establishing clinical standards for using these techniques to ensure reliability and reproducibility across diverse surgical contexts.
- Integration into Surgical Workflows: Developing portable, easy-to-use systems that seamlessly integrate into operating rooms.
- Broad Accessibility: Reducing costs and system complexity to make Surgical Optomics accessible for a wider range of healthcare settings.

Conclusion

Surgical optomics represents a groundbreaking advancement in precision surgery. By harnessing the properties of light and bespoke advanced computational methods, including machine learning, it can enable real-time visualization, characterization, and quantification of tissue and organ properties at both microscopic and macroscopic scales. Although still in the exploratory and developmental stage, this innovation has the potential to enhance surgical outcomes by facilitating precise resection of diseased tissue, minimizing collateral damage to healthy structures, and improving patient safety.

While Surgical Optomics is still in the exploratory and developmental stage, its future envisions operating rooms transformed into data-driven environments where real-time optical imaging technologies will enable the rapid interpretation of complex optical data, empowering surgeons with unprecedented insights.

As the technology advances, these tools will become more compact, faster, and seamlessly integrated into surgical workflows. However, its successful integration depends on surgeons' comprehensive understanding of these technologies and their inherent limitations. promise to enable unprecedented precision, ushering in an era of personalized, minimally invasive, and highly effective surgical interventions. Continued research and development in this field hold the potential to redefine the standard of care, enhancing patient safety and improving outcomes on a global scale. Crucially, the future application of these technologies will require seamless collaboration among surgeons, engineers, and data scientists, emphasizing the importance of interdisciplinary integration in achieving this transformative vision.

Data availability

No datasets were generated or analysed during the current study.

Received: 22 January 2025; Accepted: 23 July 2025;
Published online: 30 September 2025

References

1. Loftus, T. J. et al. Executive summary of the artificial intelligence in surgery series. *Surgery* **171**, 1435–1439 (2022).
2. de Boer, E. et al. Optical innovations in surgery. *Br. J. Surg.* **102**, e56–e72 (2015).
3. Mascagni, P. et al. New intraoperative imaging technologies: Innovating the surgeon's eye toward surgical precision. *J. Surg. Oncol.* **118**, 265–282 (2018).
4. Bannone, E. et al. Surgical optomics: hyperspectral imaging and deep learning towards precision intraoperative automatic tissue recognition-results from the EX-MACHYNA trial. *Surg. Endosc.* **38**, 3758–3772 (2024).
5. Karczewski, K. J. & Snyder, M. P. Integrative omics for health and disease. *Nat. Rev. Genet.* **19**, 299–310 (2018).
6. Ball, D. W. The electromagnetic spectrum: a history. *Spectroscopy* **22**, 14 (2007).
7. Lumen Learning & OpenStax. The Electromagnetic Spectrum in Fundamentals of Heat, Light & Sound 533–558 (NSCC, 2021).
8. Zhu, B., Rasmussen, J. C. & Sevick-Muraca, E. M. A matter of collection and detection for intraoperative and noninvasive near-infrared fluorescence molecular imaging: to see or not to see?. *Med. Phys.* **41**, 022105 (2014).
9. Lu, G. & Fei, B. Medical hyperspectral imaging: a review. *J. Biomed. Opt.* **19**, 10901 (2014).
10. Nagaya, T. et al. Fluorescence-Guided Surgery. *Front Oncol.* **7**, 314 (2017).
11. Moore, G. E. Fluorescein as an Agent in the Differentiation of Normal and Malignant Tissues. *Science* **106**, 130–131 (1947).
12. Hong, G., Antaris, A. L. & Dai H. Near-infrared fluorophores for biomedical imaging. *Nat. Biomed. Eng.* **1**, 0010 (2017).
13. Chance, B. Near-infrared images using continuous, phase-modulated, and pulsed light with quantitation of blood and blood oxygenation. *Ann. N. Y Acad. Sci.* **838**, 29–45 (1998).
14. Alander, J. T. et al. A review of indocyanine green fluorescent imaging in surgery. *Int J. Biomed. Imaging* **2012**, 940585 (2012).
15. Degett, T. H., Andersen, H. S. & Gogenur, I. Indocyanine green fluorescence angiography for intraoperative assessment of gastrointestinal anastomotic perfusion: a systematic review of clinical trials. *Langenbecks Arch. Surg.* **401**, 767–775 (2016).
16. Lin, Z., Lei, C. & Yang, L. Modern Image-Guided Surgery: A Narrative Review of Medical Image Processing and Visualization. *Sensors (Basel)* **23**, 9872 (2022).

17. Alekseev, M. et al. A study investigating the perfusion of colorectal anastomoses using fluorescence angiography: results of the FLAG randomized trial. *Colorectal Dis.* **22**, 1147–1153 (2020).
18. Galema, H. A. et al. Fluorescence-guided surgery in colorectal cancer; A review on clinical results and future perspectives. *Eur. J. Surg. Oncol.* **48**, 810–821 (2022).
19. Lutken, C. D. et al. Optimizing quantitative fluorescence angiography for visceral perfusion assessment. *Surg. Endosc.* **34**, 5223–5233 (2020).
20. Lau, N. S. et al. Current and Potential Applications for Indocyanine Green in Liver Transplantation. *Transplantation* **106**, 1339–1350 (2022).
21. Kudszus, S. et al. Intraoperative laser fluorescence angiography in colorectal surgery: a noninvasive analysis to reduce the rate of anastomotic leakage. *Langenbecks Arch. Surg.* **395**, 1025–1030 (2010).
22. Matsui, A. et al. Predicting the survival of experimental ischaemic small bowel using intraoperative near-infrared fluorescence angiography. *Br. J. Surg.* **98**, 1725–1734 (2011).
23. Jafari, M. D. et al. Perfusion assessment in laparoscopic left-sided/anterior resection (PILLAR II): a multi-institutional study. *J. Am. Coll. Surg.* **220**, 82–92 e1 (2015).
24. Ris, F. et al. Multicentre phase II trial of near-infrared imaging in elective colorectal surgery. *Br. J. Surg.* **105**, 1359–1367 (2018).
25. De Nardi, P. et al. Intraoperative angiography with indocyanine green to assess anastomosis perfusion in patients undergoing laparoscopic colorectal resection: results of a multicenter randomized controlled trial. *Surg. Endosc.* **34**, 53–60 (2020).
26. Kitai, T. et al. Fluorescence navigation with indocyanine green for detecting sentinel lymph nodes in breast cancer. *Breast Cancer* **12**, 211–215 (2005).
27. Engel, E. et al. Light-induced decomposition of indocyanine green. *Invest Ophthalmol. Vis. Sci.* **49**, 1777–1783 (2008).
28. Kedrzycki, M. S. et al. Meta-analysis Comparing Fluorescence Imaging with Radioisotope and Blue Dye-Guided Sentinel Node Identification for Breast Cancer Surgery. *Ann. Surg. Oncol.* **28**, 3738–3748 (2021).
29. Ekman, M. et al. Near-Infrared Fluorescence Image-Guided Surgery in Esophageal and Gastric Cancer Operations. *Surg. Innov.* **29**, 540–549 (2022).
30. Baiocchi, G. L. et al. Fluorescence-guided lymphadenectomy in gastric cancer: a prospective western series. *Updates Surg.* **72**, 761–772 (2020).
31. Chand, M. et al. Feasibility of fluorescence lymph node imaging in colon cancer: FLICC. *Tech. Coloproctol.* **22**, 271–277 (2018).
32. Picchetto, A. et al. Fluorescence-based sentinel lymph node mapping and lymphography evaluation: results from the IHU-IRCAD-EAES EURO-FIGS registry. *Surg. Endosc.* **37**, 5472–5481 (2023).
33. Jiang, J. X. et al. Optimization of the enhanced permeability and retention effect for near-infrared imaging of solid tumors with indocyanine green. *Am. J. Nucl. Med Mol. Imaging* **5**, 390–400 (2015).
34. Gutowski, M. et al. SGM-101: An innovative near-infrared dye-antibody conjugate that targets CEA for fluorescence-guided surgery. *Surg. Oncol.* **26**, 153–162 (2017).
35. Huang, S. W., Ou, J. J. & Wong, H. P. The use of indocyanine green imaging technique in patient with hepatocellular carcinoma. *Transl. Gastroenterol. Hepatol.* **3**, 95 (2018).
36. Blanco-Colino, R. & Espin-Basany, E. Intraoperative use of ICG fluorescence imaging to reduce the risk of anastomotic leakage in colorectal surgery: a systematic review and meta-analysis. *Tech. Coloproctol.* **22**, 15–23 (2018).
37. De Ravin, E. et al. Indocyanine green fluorescence-guided surgery in head and neck cancer: A systematic review. *Am. J. Otolaryngol.* **43**, 103570 (2022).
38. Stoffels, I. et al. Intraoperative Fluorescence Imaging for Sentinel Lymph Node Detection: Prospective Clinical Trial to Compare the Usefulness of Indocyanine Green vs Technetium Tc 99m for Identification of Sentinel Lymph Nodes. *JAMA Surg.* **150**, 617–623 (2015).
39. Wang, X. et al. Consensus Guidelines for the Use of Fluorescence Imaging in Hepatobiliary Surgery. *Ann. Surg.* **274**, 97–106 (2021).
40. Ishizawa, T. et al. Real-time identification of liver cancers by using indocyanine green fluorescent imaging. *Cancer* **115**, 2491–2504 (2009).
41. van der Vorst, J. R. et al. Near-infrared fluorescence-guided resection of colorectal liver metastases. *Cancer* **119**, 3411–3418 (2013).
42. Cassinotti, E. et al. European Association for Endoscopic Surgery (EAES) consensus on Indocyanine Green (ICG) fluorescence-guided surgery. *Surg. Endosc.* **37**, 1629–1648 (2023).
43. Diana, M. et al. Prospective Evaluation of Precision Multimodal Gallbladder Surgery Navigation: Virtual Reality, Near-infrared Fluorescence, and X-ray-based Intraoperative Cholangiography. *Ann. Surg.* **266**, 890–897 (2017).
44. Broderick, R. C. et al. Fluorescent cholangiography significantly improves patient outcomes for laparoscopic cholecystectomy. *Surg. Endosc.* **35**, 5729–5739 (2021).
45. Felli, E. et al. Laparoscopic anatomical liver resection for malignancies using positive or negative staining technique with intraoperative indocyanine green-fluorescence imaging. *HPB ((Oxf.))* **23**, 1647–1655 (2021).
46. Watanabe, J. et al. Blood Perfusion Assessment by Indocyanine Green Fluorescence Imaging for Minimally Invasive Rectal Cancer Surgery (EssentiAL trial): A Randomized Clinical Trial. *Ann. Surg.* **278**, e688–e694 (2023).
47. Safiejko, K. et al. Safety and Efficacy of Indocyanine Green in Colorectal Cancer Surgery: A Systematic Review and Meta-Analysis of 11,047 Patients. *Cancers (Basel)* **14**, 1036 (2022).
48. Deng, J. et al. Meta analysis of indocyanine green fluorescence in patients undergoing laparoscopic colorectal cancer surgery. *Front Oncol.* **12**, 1010122 (2022).
49. Trastulli, S. et al. Indocyanine green fluorescence angiography versus standard intraoperative methods for prevention of anastomotic leak in colorectal surgery: meta-analysis. *Br. J. Surg.* **108**, 359–372 (2021).
50. Mc Entee, P. D. et al. Impact of indocyanine green fluorescence angiography on surgeon action and anastomotic leak in colorectal resections. A systematic review and meta-analysis. *Surg. Endosc.* **39**, 1473–1489 (2025).
51. Xu, C. et al. A meta-analysis of short-term and long-term effects of indocyanine green fluorescence imaging in hepatectomy for liver cancer. *Photodiagnosis Photodyn. Ther.* **42**, 103497 (2023).
52. Liu, Y. et al. Meta-analysis of indocyanine green fluorescence imaging-guided laparoscopic hepatectomy. *Photodiagnosis Photodyn. Ther.* **35**, 102354 (2021).
53. Raptis, D. A. et al. Outcomes of Adult Right Graft Living Donor Liver Transplantation Utilizing the Robotic Platform-integrated Real-time Indocyanine Green Fluorescence Cholangiography Compared to the Open Approach. *Ann. Surg.* **280**, 870–878 (2024).
54. Lee, J. et al. Feasibility of indocyanine green fluorescence imaging to predict biliary complications in living donor liver transplantation: A pilot study. *Ann. Hepatobiliary Pancreat. Surg.* **29**, 32–37 (2025).
55. Hong, S. K. et al. Optimal bile duct division using real-time indocyanine green near-infrared fluorescence cholangiography during laparoscopic donor hepatectomy. *Liver Transpl.* **23**, 847–852 (2017).
56. Chu, W. et al. Anaphylactic Shock After Intravenous Administration of Indocyanine Green During Robotic Partial Nephrectomy. *Urol. Case Rep.* **12**, 37–38 (2017).

57. Bjerregaard, J., Pandia, M. P. & Jaffe, R. A. Occurrence of severe hypotension after indocyanine green injection during the intraoperative period. *A A Case Rep.* **1**, 26–30 (2013).
58. Gandaglia, G. et al. Novel Technologies in Urologic Surgery: a Rapidly Changing Scenario. *Curr. Urol. Rep.* **17**, 19 (2016).
59. Mieog, J. S. D. et al. Fundamentals and developments in fluorescence-guided cancer surgery. *Nat. Rev. Clin. Oncol.* **19**, 9–22 (2022).
60. Diana, M. et al. Intraoperative fluorescence-based enhanced reality laparoscopic real-time imaging to assess bowel perfusion at the anastomotic site in an experimental model. *Br. J. Surg.* **102**, e169–e176 (2015).
61. Diana, M. et al. Probe-based confocal laser endomicroscopy and fluorescence-based enhanced reality for real-time assessment of intestinal microcirculation in a porcine model of sigmoid ischemia. *Surg. Endosc.* **28**, 3224–3233 (2014).
62. Diana, M. et al. Real-time navigation by fluorescence-based enhanced reality for precise estimation of future anastomotic site in digestive surgery. *Surg. Endosc.* **28**, 3108–3118 (2014).
63. Diana, M. et al. Enhanced-reality video fluorescence: a real-time assessment of intestinal viability. *Ann. Surg.* **259**, 700–707 (2014).
64. AV, D. S. et al. Review of fluorescence guided surgery systems: identification of key performance capabilities beyond indocyanine green imaging. *J. Biomed. Opt.* **21**, 80901 (2016).
65. Gioux, S., Choi, H. S. & Frangioni, J. V. Image-guided surgery using invisible near-infrared light: fundamentals of clinical translation. *Mol. Imaging* **9**, 237–255 (2010).
66. Hardy, N. P. et al. Inter-user variation in the interpretation of near infrared perfusion imaging using indocyanine green in colorectal surgery. *Surg. Endosc.* **35**, 7074–7081 (2021).
67. Vallance, A. et al. A collaborative review of the current concepts and challenges of anastomotic leaks in colorectal surgery. *Colorectal Dis.* **19**, O1–O12 (2017).
68. Karampinis, I. et al. Indocyanine Green Tissue Angiography Can Reduce Extended Bowel Resections in Acute Mesenteric Ischemia. *J. Gastrointest. Surg.* **22**, 2117–2124 (2018).
69. van den Bos, J. et al. Near-Infrared Fluorescence Imaging for Real-Time Intraoperative Guidance in Anastomotic Colorectal Surgery: A Systematic Review of Literature. *J. Laparoendosc. Adv. Surg. Tech. A* **28**, 157–167 (2018).
70. Faber, R. A. et al. Indocyanine green near-infrared fluorescence bowel perfusion assessment to prevent anastomotic leakage in minimally invasive colorectal surgery (AVOID): a multicentre, randomised, controlled, phase 3 trial. *Lancet Gastroenterol. Hepatol.* **9**, 924–934 (2024).
71. Hoogstins, C. et al. Setting Standards for Reporting and Quantification in Fluorescence-Guided Surgery. *Mol. Imaging Biol.* **21**, 11–18 (2019).
72. Ashoka, A. H. et al. Near-infrared fluorescent coatings of medical devices for image-guided surgery. *Biomaterials* **261**, 120306 (2020).
73. Goncalves, L. N. et al. Perfusion Parameters in Near-Infrared Fluorescence Imaging with Indocyanine Green: A Systematic Review of the Literature. *Life (Basel)* **11**, 433 (2021).
74. Wada, T. et al. ICG fluorescence imaging for quantitative evaluation of colonic perfusion in laparoscopic colorectal surgery. *Surg. Endosc.* **31**, 4184–4193 (2017).
75. Diana, M. et al. Reply to Letter: "Enhanced Reality Fluorescence Videography to Assess Bowel Perfusion: The Cybernetic Eye". *Ann. Surg.* **265**, e49–e52 (2017).
76. Diana, M. et al. Precision real-time evaluation of bowel perfusion: accuracy of confocal endomicroscopy assessment of stoma in a controlled hemorrhagic shock model. *Surg. Endosc.* **31**, 680–691 (2017).
77. Quero, G. et al. Discrimination between arterial and venous bowel ischemia by computer-assisted analysis of the fluorescent signal. *Surg. Endosc.* **33**, 1988–1997 (2019).
78. D'Urso, A. et al. Computer-assisted quantification and visualization of bowel perfusion using fluorescence-based enhanced reality in left-sided colonic resections. *Surg. Endosc.* **35**, 4321–4331 (2021).
79. Barberio, M. et al. Quantitative fluorescence angiography versus hyperspectral imaging to assess bowel ischemia: A comparative study in enhanced reality. *Surgery* **168**, 178–184 (2020).
80. Kong, W. et al. Quantitative evaluation of anastomotic perfusion during colorectal surgery via indocyanine green fluorescence angiography: a narrative review. *Ann. Transl. Med.* **10**, 1402 (2022).
81. Cahill, R. A. et al. Artificial intelligence indocyanine green (ICG) perfusion for colorectal cancer intra-operative tissue classification. *Br. J. Surg.* **108**, 5–9 (2021).
82. Moynihan, A. et al. CLASSICA: Validating artificial intelligence in classifying cancer in real time during surgery. *Colorectal Dis.* **25**, 2392–2402 (2023).
83. Wu, X. et al. In vivo and in situ tracking cancer chemotherapy by highly photostable NIR fluorescent theranostic prodrug. *J. Am. Chem. Soc.* **136**, 3579–3588 (2014).
84. Wang, K. et al. Fluorescence image-guided tumour surgery. *Nat. Rev. Bioeng.* **1**, 161–179 (2023).
85. Lee, J. Y. K. et al. Review of clinical trials in intraoperative molecular imaging during cancer surgery. *J. Biomed. Opt.* **24**, 1–8 (2019).
86. Staderini, M. et al. Peptides for optical medical imaging and steps towards therapy. *Bioorg. Med. Chem.* **26**, 2816–2826 (2018).
87. Achterberg, F. B. et al. Clinical translation and implementation of optical imaging agents for precision image-guided cancer surgery. *Eur. J. Nucl. Med. Mol. Imaging* **48**, 332–339 (2021).
88. Hentzen, J. et al. Molecular fluorescence-guided surgery of peritoneal carcinomatosis of colorectal origin: A narrative review. *J. Surg. Oncol.* **118**, 332–343 (2018).
89. Gabriels, R. Y. et al. Detection of Early Esophageal Neoplastic Barrett Lesions with Quantified Fluorescence Molecular Endoscopy Using Cetuximab-800CW. *J. Nucl. Med.* **64**, 803–808 (2023).
90. Tjalma, J. J. J. et al. Quantitative fluorescence endoscopy: an innovative endoscopy approach to evaluate neoadjuvant treatment response in locally advanced rectal cancer. *Gut* **69**, 406–410 (2020).
91. Hernot, S. et al. Latest developments in molecular tracers for fluorescence image-guided cancer surgery. *Lancet Oncol.* **20**, e354–e367 (2019).
92. Falco, J. et al. Cutting Edge in Thyroid Surgery: Autofluorescence of Parathyroid Glands. *J. Am. Coll. Surg.* **223**, 374–380 (2016).
93. Falco, J. et al. Increased identification of parathyroid glands using near infrared light during thyroid and parathyroid surgery. *Surg. Endosc.* **31**, 3737–3742 (2017).
94. Shenson, J. A. et al. Multispectral Imaging for Automated Tissue Identification of Normal Human Surgical Specimens. *Otolaryngol. Head. Neck Surg.* **164**, 328–335 (2021).
95. Nouri, D., Lucas, Y. & Treuillet, S. Hyperspectral interventional imaging for enhanced tissue visualization and discrimination combining band selection methods. *Int J. Comput Assist Radio. Surg.* **11**, 2185–2197 (2016).
96. Jacques, S. L. Corrigendum: Optical properties of biological tissues: a review. *Phys. Med. Biol.* **58**, 5007–5008 (2013).
97. Akbari, H. & Kosugi, Y. Hyperspectral Imaging: a New Modality in Surgery. *in Recent Advances in Biomedical Engineering*, (2009).
98. Clancy, N. T. et al. Surgical spectral imaging. *Med Image Anal.* **63**, 101699 (2020).
99. Zahra, A. et al. Current advances in imaging spectroscopy and its state-of-the-art applications. *Expert Sys. Appl.* **238**, 122172 (2024).
100. Li, Q. et al. Review of spectral imaging technology in biomedical engineering: achievements and challenges. *J. Biomed. Opt.* **18**, 100901 (2013).
101. Shapey, J. et al. Intraoperative multispectral and hyperspectral label-free imaging: A systematic review of in vivo clinical studies. *J. Biophotonics* **12**, e201800455 (2019).

102. Chiang, N. et al. Evaluation of hyperspectral imaging technology in patients with peripheral vascular disease. *J. Vasc. Surg.* **66**, 1192–1201 (2017).
103. Kulcke, A. et al. A compact hyperspectral camera for measurement of perfusion parameters in medicine. *Biomed. Tech. ((Berl.))* **63**, 519–527 (2018).
104. Chin, M. S. et al. Hyperspectral Imaging for Burn Depth Assessment in an Animal Model. *Plast. Reconstr. Surg. Glob. Open* **3**, e591 (2015).
105. Sicher, C. et al. Hyperspectral imaging as a possible tool for visualization of changes in hemoglobin oxygenation in patients with deficient hemodynamics - proof of concept. *Biomed. Tech. Berl.* **63**, 609–616 (2018).
106. Ayala, L. et al. Abstract: Multispectral Imaging Enables Visualization of Spreading Depolarizations in Gyrencephalic Brain, in *Bildverarbeitung für die Medizin 2019*. 2019. p. 244–244.
107. Wirkert, S. J. et al. Domain and task specific multispectral band selection (Conference Presentation). *in Design and Quality for Biomedical Technologies XI*, (2018).
108. Sorg, B. S. et al. Hyperspectral imaging of hemoglobin saturation in tumor microvasculature and tumor hypoxia development. *J. Biomed. Opt.* **10**, 44004 (2005).
109. Ayala, L. et al. Spectral imaging enables contrast agent-free real-time ischemia monitoring in laparoscopic surgery. *Sci. Adv.* **9**, eadd6778 (2023).
110. Köhler, H. et al. Evaluation of hyperspectral imaging (HSI) for the measurement of ischemic conditioning effects of the gastric conduit during esophagectomy. *Surgical Endosc.* **33**, 3775–3782 (2019).
111. Jansen-Winkeln, B. et al. Comparison of hyperspectral imaging and fluorescence angiography for the determination of the transection margin in colorectal resections-a comparative study. *Int J. Colorectal Dis.* **36**, 283–291 (2021).
112. Pfahl, A. et al. Combined indocyanine green and quantitative perfusion assessment with hyperspectral imaging during colorectal resections. *Biomed. Opt. Express* **13**, 3145–3160 (2022).
113. Clancy, N. T. et al. Intraoperative colon perfusion assessment using multispectral imaging. *Biomed. Opt. Express* **12**, 7556–7567 (2021).
114. Tetschke, F. et al. Hyperspectral imaging for monitoring oxygen saturation levels during normothermic kidney perfusion. *J. Sens. Sens. Syst.* **5**, 313–318 (2016).
115. Holzer, M. S. et al. Assessment of renal oxygenation during partial nephrectomy using hyperspectral imaging. *J. Urol.* **186**, 400–404 (2011).
116. Dietrich, M. et al. Hyperspectral imaging for perioperative monitoring of microcirculatory tissue oxygenation and tissue water content in pancreatic surgery - an observational clinical pilot study. *Perioper. Med. ((Lond.))* **10**, 42 (2021).
117. Zuzak, K. J. et al. Characterization of a near-infrared laparoscopic hyperspectral imaging system for minimally invasive surgery. *Anal. Chem.* **79**, 4709–4715 (2007).
118. Cervantes-Sanchez, F. et al. Automatic tissue segmentation of hyperspectral images in liver and head neck surgeries using machine learning. *Artificial Intelligence Surgery,* (2021).
119. Fabelo, H. et al. Spatio-spectral classification of hyperspectral images for brain cancer detection during surgical operations. *PLoS One* **13**, e0193721 (2018).
120. Fabelo, H. et al. In-VivoHyperspectral Human Brain Image Database for Brain Cancer Detection. *IEEE Access* **7**, 39098–39116 (2019).
121. Felli, E. et al. Automatic Liver Viability Scoring with Deep Learning and Hyperspectral Imaging. Di*agnostics (Basel),***11 (**2021).
122. Collins, T. et al. Automatic optical biopsy for colorectal cancer using hyperspectral imaging and artificial neural networks. *Surg. Endosc.* **36**, 8549–8559 (2022).
123. Studier-Fischer, A. et al. Spectral organ fingerprints for machine learning-based intraoperative tissue classification with hyperspectral imaging in a porcine model. *Sci. Rep.* **12**, 11028 (2022).
124. Seidlitz, S. et al. Robust deep learning-based semantic organ segmentation in hyperspectral images. *Med Image Anal.* **80**, 102488 (2022).
125. Sellner, J. et al. Xeno-learning: knowledge transfer across species in deep learning-based spectral image analysis. arXiv:2410.19789 https://doi.org/10.48550/arXiv.2410.19789 (2024).
126. Barberio, M. et al. Deep Learning Analysis of In Vivo Hyperspectral Images for Automated Intraoperative Nerve Detection. *Diagnostics (Basel)* **11,** 1508 (2021).
127. Okamoto, N. et al. Computer-Assisted Differentiation between Colon-Mesocolon and Retroperitoneum Using Hyperspectral Imaging (HSI) Technology. *Diagnostics (Basel)* **12**, 2225 (2022).
128. Chalopin, C. et al. [Artificial intelligence and hyperspectral imaging for image-guided assistance in minimally invasive surgery]. *Chirurgie (Heidelb.)* **93**, 940–947 (2022).
129. Tufan, K. & Belli, A. K. Analysis of nervous fiber, muscle, and blood vessels using their ulraviolet near infrared reflectance characteristics. *Biomed. Mater. Eng.* **26**, S2179–S2185 (2015).
130. Ernstberger, M. et al. Spectrophotometric measurements of human tissues for the detection of subjacent blood vessels in an endonasal endoscopic surgical approach. *J. Biophotonics* **6**, 310–313 (2013).
131. Hanahan, D. & Weinberg, R. A. Hallmarks of cancer: the next generation. *Cell* **144**, 646–674 (2011).
132. Pandey, R. et al. AI-Powered Biomolecular-Specific and Label-Free Multispectral Imaging Rapidly Detects Malignant Neoplasm in Surgically Excised Breast Tissue Specimens. *Arch. Pathol. Lab Med* **147**, 1298–1306 (2023).
133. Leon, R. et al. Hyperspectral imaging benchmark based on machine learning for intraoperative brain tumour detection. *NPJ Precis Oncol.* **7**, 119 (2023).
134. Hu, Z. et al. First-in-human liver-tumour surgery guided by multispectral fluorescence imaging in the visible and near-infrared-I/II windows. *Nat. Biomed. Eng.* **4**, 259–271 (2020).
135. Jansen-Winkeln, B. et al. Feedforward Artificial Neural Network-Based Colorectal Cancer Detection Using Hyperspectral Imaging: A Step towards Automatic Optical Biopsy. *Cancers (Basel)* **13**, 967 (2021).
136. Collins, T. et al. Automatic Recognition of Colon and Esophagogastric Cancer with Machine Learning and Hyperspectral Imaging. *Diagnostics (Basel)* **11**, 1810 (2021).
137. De Landro, M. et al. Hyperspectral Imagery for Assessing Laser-Induced Thermal State Change in Liver. *Sensors (Basel)* **21**, 643 (2021).
138. Danilov, V. V. et al. Advancing laser ablation assessment in hyperspectral imaging through machine learning. *Comput Biol. Med.* **179**, 108849 (2024).
139. De Landro, M. et al. Prediction of In Vivo Laser-Induced Thermal Damage with Hyperspectral Imaging Using Deep Learning. *Sensors (Basel)* **21**, 6934 (2021).
140. Famularo, S. et al. Partial Hepatic Vein Occlusion and Venous Congestion in Liver Exploration Using a Hyperspectral Camera: A Proposal for Monitoring Intraoperative Liver Perfusion. *Cancers (Basel)*, **15**, 2397 (2023).
141. Felli, E. et al. Hyperspectral Imaging in Major Hepatectomies: Preliminary Results from the Ex-Machyna Trial. *Cancers (Basel)* **14**, 5591 (2022).
142. Barberio, M. et al. Intraoperative Guidance Using Hyperspectral Imaging: A Review for Surgeons. *Diagnostics (Basel)*, **11**, 2066 (2021).
143. Baker, W. B. et al. Modified Beer-Lambert law for blood flow. *Biomed. Opt. Express* **5**, 4053–4075 (2014).

144. Holmer, A. et al. Hyperspectral imaging in perfusion and wound diagnostics - methods and algorithms for the determination of tissue parameters. *Biomed. Tech. Berl*. **63**, 547–556 (2018).
145. Konugolu Venkata Sekar, S. et al. Broadband Time Domain Diffuse Optical Reflectance Spectroscopy: A Review of Systems, Methods, and Applications. *Appl. Sci.* **9**, 5465 (2019).
146. Borycki, D., Kholiqov, O. & Srinivasan, V. J. Reflectance-mode interferometric near-infrared spectroscopy quantifies brain absorption, scattering, and blood flow index in vivo. *Opt. Lett.* **42**, 591–594 (2017).
147. Sutin, J. et al. Time-domain diffuse correlation spectroscopy. *Optica* **3**, 1006–1013 (2016).
148. Muller, D. & Kramer, F. MIScnn: a framework for medical image segmentation with convolutional neural networks and deep learning. *BMC Med Imaging* **21**, 12 (2021).
149. Wirkert, S. J. et al. Robust near real-time estimation of physiological parameters from megapixel multispectral images with inverse Monte Carlo and random forest regression. *Int J. Comput. Assist. Radio. Surg.* **11**, 909–917 (2016).
150. Wirkert, S. J. et al. Physiological Parameter Estimation from Multispectral Images Unleashed. (2017).
151. Ayala, L. A. et al. Live Monitoring of Haemodynamic Changes with Multispectral Image Analysis. (2019).
152. Seidlitz, S. et al. New spectral imaging biomarkers for sepsis and mortality in intensive care. arXiv:2408.09873 https://doi.org/10.48550/arXiv.2408.09873 (2024).
153. Studier-Fischer, A. et al. HeiPorSPECTRAL - the Heidelberg Porcine HyperSPECTRAL Imaging Dataset of 20 Physiological Organs. *Sci. Data* **10**, 414 (2023).
154. Ayala, L. et al. The SPECTRAL Perfusion Arm Clamping dAtaset (SPECTRALPACA) for video-rate functional imaging of the skin. *Sci. Data* **11**, 536 (2024).
155. Cui, R. et al. Deep Learning in Medical Hyperspectral Images: A Review. *Sensors (Basel)*, **22**, 9790 (2022).
156. Geirhos, R. et al. Shortcut learning in deep neural networks. *Nat. Mach. Intell.* **2**, 665–673 (2020).
157. Qasim, A. B. et al. Test-time augmentation with synthetic data addresses distribution shifts in spectral imaging. *Int. J. Comput. Assist. Radio. Surg.* **19**, 1021–1031 (2024).
158. Baumann, A. et al. Deep intra-operative illumination calibration of hyperspectral cameras. *Lect. Notes Comput.* Sci. **15006**, 120–131 (2024).
159. Pruitt, K. et al. A High-Speed Hyperspectral Laparoscopic Imaging System. *Proc. SPIE Int. Soc. Opt Eng*. 12466 (2023).
160. Ayala, L., Light source calibration for multispectral imaging in surgery. *Int. J. Comput. Assisted Radiology Surgery* (2020).
161. Bigio, I. J. and S. Fantini, *Quantitative Biomedical Optics*. 2018.
162. Cuccia, D. J. et al. Quantitation and mapping of tissue optical properties using modulated imaging. *J. Biomed. Opt.* **14**, 024012 (2009).
163. Gioux, S., Mazhar, A. & Cuccia, D. J. Spatial frequency domain imaging in 2019: principles, applications, and perspectives. *J. Biomed. Opt.* **24**, 1–18 (2019).
164. Saager, R. B., Cuccia, D. J., Saggese, S., Kelly, K. M. & Durkin, A. J. A light emitting diode (led) based spatial frequency domain imaging system for optimization of photodynamic therapy of nonmelanoma skin cancer: Quantitative reflectance imaging. *Lasers Surg. Med.* **45**, 207–215 (2013).
165. Nguyen, T. T. et al. Novel application of a spatial frequency domain imaging system to determine signature spectral differences between infected and noninfected burn wounds. *J. Burn Care Res* **34**, 44–50 (2013).
166. Rohrbach, D. J. et al. Preoperative mapping of nonmelanoma skin cancer using spatial frequency domain and ultrasound imaging. *Acad. Radio.* **21**, 263–270 (2014).
167. Nandy, S. et al. Characterizing optical properties and spatial heterogeneity of human ovarian tissue using spatial frequency domain imaging. *J. Biomed. Opt.* **21**, 101402 (2016).
168. Wirth, D. et al. Feasibility of using spatial frequency-domain imaging intraoperatively during tumor resection. *J. Biomed. Opt.* **24**, 1–6 (2018).
169. Ponticorvo, A. et al. Quantitative assessment of graded burn wounds in a porcine model using spatial frequency domain imaging (SFDI) and laser speckle imaging (LSI). *Biomed. Opt. Express* **5**, 3467–3481 (2014).
170. Gioux, S. et al. First-in-human pilot study of a spatial frequency domain oxygenation imaging system. *J. Biomed. Opt.* **16**, 086015 (2011).
171. Yafi, A. et al. Quantitative skin assessment using spatial frequency domain imaging (SFDI) in patients with or at high risk for pressure ulcers. *Lasers Surg. Med.* **49**, 827–834 (2017).
172. van de Giessen, M., Angelo, J. P. & Gioux, S. Real-time, profile-corrected single snapshot imaging of optical properties. *Biomed. Opt. Express* **6**, 4051–4062 (2015).
173. Ségaud, S. et al. Trident: A dual oxygenation and fluorescence imaging platform for real-time and quantitative surgical guidance. *Front. Photon.* **3** (2022).
174. Cinelli, L. et al. Single Snapshot Imaging of Optical Properties (SSOP) for Perfusion Assessment during Gastric Conduit Creation for Esophagectomy: An Experimental Study on Pigs. *Cancers* (Basel), **13** (2021).
175. Rodriguez-Luna, M. R. et al. Quantification of bowel ischaemia using real-time multispectral Single Snapshot Imaging of Optical Properties (SSOP). *Surg. Endosc.* **37**, 2395–2403 (2023).
176. Aguenounon, E. et al. Real-time, wide-field and high-quality single snapshot imaging of optical properties with profile correction using deep learning. *Biomed. Opt. Express* **11**, 5701–5716 (2020).
177. Vervandier, J. & Gioux, S. Single snapshot imaging of optical properties. *Biomed. Opt. Express* **4**, 2938–2944 (2013).
178. Schmidt, M. et al. Real-time, wide-field, and quantitative oxygenation imaging using spatiotemporal modulation of light. *J. Biomed. Opt.* **24**, 1–7 (2019).
179. Legrand, M. et al. Full field elastography using deep learning approach, in *Tissue Optics and Photonics III*. 43 (2024).
180. Gunalan, A. & Mattos, L. S. Towards OCT-Guided Endoscopic Laser Surgery-A Review. *Diagnostics (Basel)* **13**, 677 (2023).
181. Seromenho, E. M. et al. Single-shot off-axis full-field optical coherence tomography. *Appl. Phys. Lett.* **121**, 113702 (2022).
182. Santos, I. P. et al. Raman spectroscopy for cancer detection and cancer surgery guidance: translation to the clinics. *Analyst* **142**, 3025–3047 (2017).
183. Chen, Q. Y. et al. Indocyanine green fluorescence imaging-guided versus conventional laparoscopic lymphadenectomy for gastric cancer: long-term outcomes of a phase 3 randomised clinical trial. *Nat. Commun.* **14**, 7413 (2023).
184. Fadel, M. G. et al. Efficacy and Safety of Fluorescence-Guided Surgery Compared to Conventional Surgery in the Management of Colorectal Cancer: A Systematic Review and Meta-Analysis. *Cancers (Basel)*, **16**, 3377 (2024).

Acknowledgements

Funded by the European Union (GA 101072354). Views and opinions expressed are however those of the author(s) only and do not necessarily reflect those of the European Union or the European Research Executive Agency. Neither the European Union nor the granting authority can be held responsible for them.

Author contributions

G.S. and E.B. contributed equally to this work. G.S., E.B. and M.D.: Conceptualization G.S., E.B., S.S., M.H., L.B. and A.P.:

Writing – Original Draft Preparation S.L., F.T., M.C., S.G., L.M. and M.D.: Supervision, Writing – Review & Editing. All authors have read and approved the manuscript.

Competing interests

L.B., A.P. and S.G. are Full-time employees of Intuitive Surgical. All other authors declare no financial competing interests.

Additional information

Correspondence and requests for materials should be addressed to Michele Diana.

Reprints and permissions information is available at http://www.nature.com/reprints

Publisher's note Springer Nature remains neutral with regard to jurisdictional claims in published maps and institutional affiliations.